Investigation of structural and optical properties of mixed phase nanoparticles titania synthesized by simple sol gel process

Rezika Zedek, Hatem Djedjiga, Mohamed Megherbi, Mohammed *Said Belkaid*

Laboratory of Advanced Technologies of Electrical Engineering (LATAGE), Faculty of Electrical Engineering and Computer science, Mouloud Mammeri University(UMMTO), BP 17 RP, 15000 *Tizi-Ouzou, Algeria*

rezika.zedek2010@yahoo.fr

Abstract

The purpose of this study is to calculate the band gap value of mixture phases of TiO_2 nanoparticless. The direct and indirect band gap of the samples can be estimated from measurements data of diffuse reflectance spectrascopy. Iron-doped titanium dioxide (TiO_2) nanoparticles were prepared via a facile and economical sol gel procedure. The prepared samples were characterized using X-ray diffraction (XRD) and UV-Vis diffuse reflectance spectroscopy. The obtained results by DRX displayed that samples annealed at 550 °C for 3h crystallized into mixture phases. The optical properties were investigated by UV-vis diffuse reflectance spectra (DRS). Using the DRS data, direct and indirect bandgap of the samples was determined by applying the Kubelka–Munk (K-M) equation. Graphics representations were used to calculate Eg: F(R) versus hv, F(R) versus λ, $(F(R)\ h\nu)^{\wedge n}$ versus hv with n = ½ for an indirect allowed transition and n = 2 for a direct allowed transition). Moreover the UV-Vis light-diffuse reflectance spectroscopy analysis depicted that the absorption region of Fe-doped TiO_2 was shifted to the visible-light range, which was attributed to incorporation of iron into the TiO_2 lattice during chemical reaction.

Keywords Titanium Dioxide, Mixture Phases, Kubelka–Munk Function, Absorbance Spectra, Direct and Indirect Band Gap Energy.

1. Introduction

Nanocrystalline transition metal oxide (TiO_2) is functional in a large range of industrial applications that include photocatalysis [1], solar cell [2-4], pigments and gas sensors [5]. It is the most extensively used oxide in some applications owing to its abundance [6], low cost, high efficiency, stability, nontoxicity and excellent biocompatibility [7-10]. The chemical and physical properties of nanomaterial are strongly influenced by the size crystallite, shape and crystalline phases. Recently, extensive researches have been conducted on the fabrication and characterization of TiO_2 nanoparticles because of their novel properties in large field application. TiO_2 has three kinds of phases, anatase (tetragonal), rutile (tetragonal), and brookite (orthorhombic) [11]. Gupta and Tripathi

signaled that the brookite is the rarest of the natural TiO_2 polymorphs and is the most difficult phase to prepare in the laboratory. Additionally, the different crystallographic orientations of the same material may exhibit different activities. For instance, from the catalytic viewpoint, anatase and rutile are the most important phase. On the other hand, TiO_2 is practically no moving in visible light due to its wide band gap energy, the anatase phase has a band gap of 3.2 eV (385 nm), while the rutile phase has a smaller band gap of 3.0 eV (410 nm) [12, 4]. Additionally, the anatase can show a photocatalytic activity only under UV light irradiation, while UV light accounts for only a small fraction (~5%) of the solar energy [13]. Therefore, band gap engineering by possible modification of materials is one of the moving investigate. Paul et Choudhury [14] demonstrated that pure anatase and rutile phase have band gap in the UV region, whereas a mixture of these phases has lower band gap and corresponds to the visible region. They indicate that the mixed phase nanocristalline titania exhibit superior photocatalytic activity, this is due to the synergitic effect of mixed phases [14]. Biswajit et Amarjyoti [15] reported that the crystalline anatase and pure rutile TiO_2 have band gap in UV region with short carrier lifetime, in contrast the mixture of these phases have lower band gap and longer decay time. Additionnally they displayed that in mixed phase TiO_2 the charge carriers are separated due to the transfer of electrons from anatase to rutile. Hurum et al [16] indicated that the presence of rutile phase extends the photoactive response to the visible region, harvesting more light, and stabilization of charge separation by electron transfer from rutile to anatase trapping sites slows down the recombination. Yamada et al [17] reported that the anatase phase has an indirect band gap, the conduction band electron and valence band hole will be in different position in the Brillouin zone, whereas the rutile phase has a direct band gap. In principal the band gap energy depends strongly the structure crystals. The mixture of TiO_2 NPs has

reduced band gap because of the presence of interface defects and due to the different alignment of the band states in anatase and rutile. Recently, Biswajit et Amarjyoti, Baiju et al [32,18] reported that the anatase-rutile mixture phase is found to have a magical effect on the charge transfer process, and longer carrier lifetime, whereas a short lifetime is reported when rutile content increases. Su et al. [19] reported that a mixture of 60 % anatase and 40 % rutile mixed phase TiO_2 exhibit better photoactivity than individual anatase or rutile polymorphs.

Diverse method have been introduced to prepare metal ion-doped TiO_2 nanoparticles are the hydrothermal method [20], sol-gel method [21-23], thermal hydrolysis [24],wet chemical synthesis and anodic- oxidation [25-26]. Among these methods, the sol–gel method represents several advantages over other methods are reported in literature.
In this present investigation, titania nanoparticles were developed by standard sol gel process and were characterized using XRD and UV-Vis diffuse reflectance spectroscopy. The principal goal of this paper is to determine an important direct and indirect optical band gap of mixture phases using Kabelka-Munk method.

2. Experimental part

2.1. Preparation of Undoped and Doped TiO_2 Nanoparticles

The experimental process for the synthesis of pure and Fe-doped TiO_2 nanoparticles was prepared by dissolving TTIP into ethanol under vigorous magnetic stirring for 1 hour at temperature of 70°C and followed by adding 2ml EG used as stabillizer. For a doping process, appropriate amount of iron sulfate hyperahydrate ($FeSO_4.7H_2O$) was added and stirred until a homogeneous solution precursor was obtained. The solution was dried at 70 °C for 3 hours, and then air cooled to room temperature. The samples powders were collected by suction filtration and washed by deionized water (about 60ml). The dried gel was grinded using a motar and calcined in a muffle furnace at 550◦C for 3 h. The samples of Fe doped and undoped TiO_2 nanoparticles were obtained by Sol Gel technique. Synthesis procedure for iron doped TiO_2 is schematically shown in Fig.1

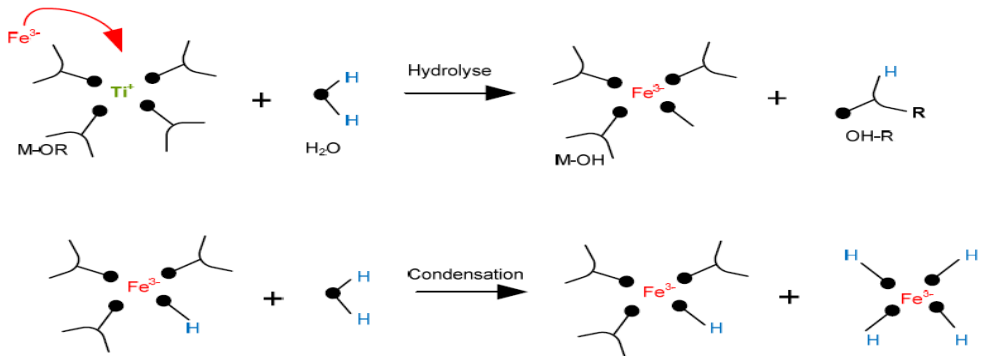

Fig. 1.Synthesis of Fe doped TiO_2 by Sol-Gel method.

2.2. Band gap energy

The band gap energy (Eg) is an essential parameter in semiconductor physics. The band gap is indicated by the region of strong absorption. Tauc proposed a method to estimate the optical band gap energy using data absorption spectra [27]. Subsequently, this method was developed by Davis and Mott [28]. In the Tauc method, the density of states is assumed to be parabolic, so that it can be linearized by a square-root function. In a simplified way, Eg is evaluated from the plot obtained between the highest valence band edge and the lowest conduction band edge. Electrons in a solid Occupy allowed energy bands separated by forbidden energy gaps. Two types of band-to-band transitions are suggested:

- Direct transitions (n = 2) when the participation of a phonon is not required to conserve momentum Fig.2 (a).
- Indirect transitions (n = 1/2) when at least one phonon participates in the absorption or emission of a phonon in order to conserve momentum Fig.2 (b).

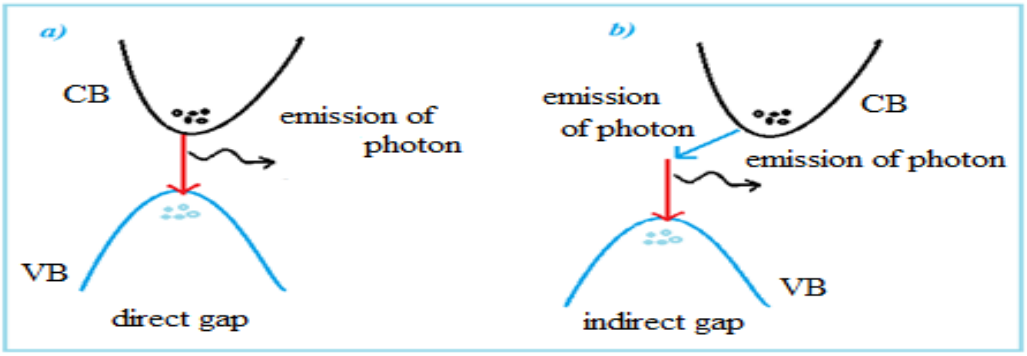

Fig. 2. Simplified representation of the band transition: (a) Direct gap, (b) Indirect gap

2.3. Measurements.

X-Ray diffraction (XRD) analysis was performed using a Bruker D8 Advanced two-circle Diffractometer with Cu-Kα (λ = 1.54021 Å) °) equiped with a Ge(111) monochromator and a Lynx Eye detector with an accelerating voltage of 40 kV and current of 40 mA (A) and scan speed 6°.min^{-} over the range of 2θ from 20 °C to 80°C and UV–vis diffuse reflectance spectroscopy was collected from ranging 200-800 nm with a resolution of 1.0 nm. The spectra were used to determine the optical proprieties

3. Result and discussion

➢ Phase identification by DRX

X-Ray Diffraction (XRD) analysis was carried out on TiO_2 NPs prepared by simple sol gel process.

The X-ray diffraction pattern of the prepared titania nanoparticles annealing at 550 °C for 3 h is depicted in Fig.3. Before annealing, the samples show the amorphous structure as shown in Fig.3a). This structure was converted into a crystalline structure after annealing as shown in Fig.3(b) and Fig.3(c). The results reveal the presence of mixture (anatase and rutile) phases with (101) and (110) main crystallographic orientations respectively. Angles corresponding to anatase are at 25.39, 37.91, 48.25, 62.7, 70.2 and 75.09, with peaks (101), (004), (200), (204), (220) and (215), respectively (ICSD no. 96-900-8214). While rutile phases 27.61, 36.25, 41, 32 and 56.69 are indicated as the (110), (101), (111) and (220) planes respectively.

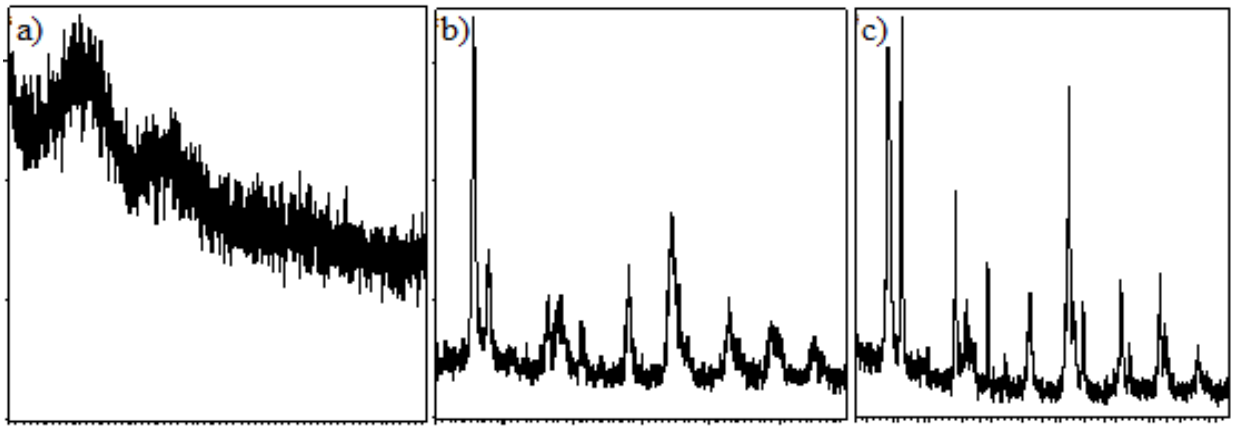

Fig 3. The XRD patterns of a) amorphous structure (before annealing) b) and c) of undoped and Fe-doped TiO_2 nanoparticles (after annealing at 550°C for 3h).

For TiO_2 NPs crystal system, the lattice parameters (a=b≠c) were estimated from 2θ values of XRD pattern using Bragg's law (Table 1). The lattice constants do not change with the presence of Fe

doping in the crystal TiO_2. The results of lattice parameters of pure and Fe^{3+}-doped-TiO_2 are presented in **Table 1**.

Table 1: lattice parameters of pure and Fe doped TiO_2 nanoparticles

Samples	Un-doped TiO_2	Fe-doped TiO_2
Anatase (2θ)	25.39(101) 48.25(200)	25.39(101) 48.22 (200)
Rutile (2θ)	27.50(110) 36.20(101)	27.52(110) 36.19(101)
Lattice parameters a=b ≠c(A°)(Bragg's law)	Anatase; a=b=3.55, c=9.00 Rutile; a=b=4.31, c=2.78	Anatase; a=b=3.56, c=8.96 Rutile; a=b=4.27, c=2.77

The mass fractions of the samples is calculated by the following formula **[30]** and presented in **Table 2**.

$$fr = \frac{Ir}{0.886\,Ia + Ir} \quad \text{..... (1)}$$

$$fa = \frac{0.886\,Ia}{0.886\,Ia + Ir} \quad \text{..... (2)}$$

Where fr and fa represent the weight percent of rutile TiO_2 and anatase TiO_2, respectively. I_a and I_r integrated diffraction intensities of the most intense anatase (101) and rutile (110) peaks, respectively. The parameters calculated using Eqs. **(1)** and **(2)** are depicted in **Table 2**

	(101) Anatase phase (%)	(110)Rutile phase (%)
Pure TiO_2	(25.39)81.86	(27.50)18.13
Fe-TiO_2	(25.39)18.42	(27.50)81.88

Table 2: the mass fractions of rutile and anatase phases in the samples

➢ Optical study by DRS

Data measurements of diffuse reflectance spectroscopy (DRS) have been performed to analyze the optical properties of undoped and Fe-doped TiO_2 NPs. The diffuse reflectance spectroscopy DRS is one of the most employed technique for the determination of the optical parameters such as absorbance spectra, bandgap direct and indirect of the material. The main goal of this part is to evaluate the result of the UV–vis diffuse reflectance spectroscopy, the application of the Kubelka–Munk theory and Tauc plot equation for the estimation of the optical bandgap direct and indirect of mixture TiO_2 NPs. The UV–vis absorption spectral of doped and TiO_2 pristine is carried out in diffuse reflectance mode (DRS). The reflectance of the samples is converted to absorbance by Kubelka–Munk function noted F(R) and given by **[29]**

$$F(R) = \frac{K}{S} = \frac{(1-R)^2}{2R} \quad \text{.....(3)}$$

Where F(R) is known Kabelka-Munk function, K is the molar absorption coefficient, S is scattering factor and R is the reflectance of TiO_2 NPs and is equal to:

$$\%R = \frac{R}{100} \quad \text{.....(4)}$$

The estimation of the band gap energy of the mixture phases by applying the Kubelka–Munk (F(R)) has been reported by Kubelka P **[31].** They have also signaled that the calculation of band gap value for TiO_2 by directly plotting F(R) against **hv** or **λ**. The absoption spectra of TiO_2 NPs are shown in **Fig. 4**. The optical band gap of undoped and doped TiO_2 were estimated around 440 nm (2.81eV) and 489.6nm (2.53 eV) by ploting F(R) versus photon energy hv. In all the cases, the optical edge or gap was inferred by linear extrapolation of the absorbance from the high slope region obtained from the spectra.

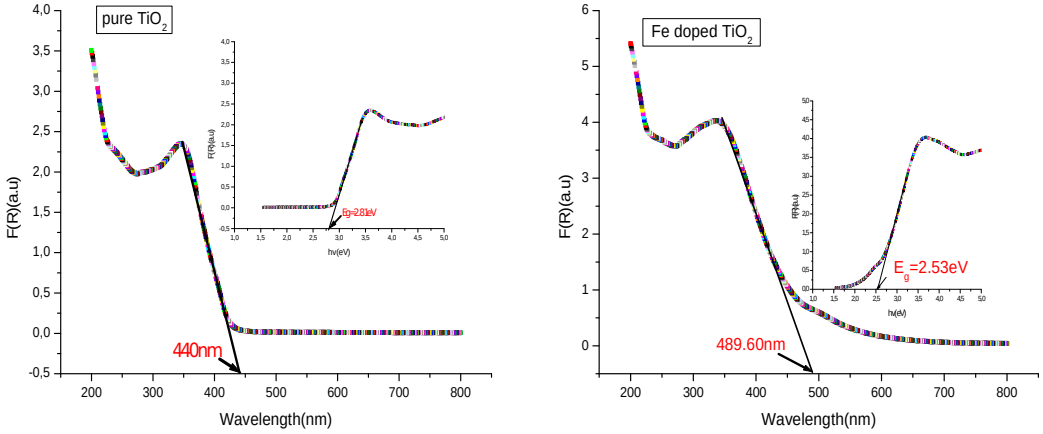

Fig. 4. Absorption spectra of undoped and doped TiO_2NPs

The Kubelka–Munk function can be modified by multiplying the F(R) by the incident photon energy (hv), using the corresponding coefficient (**n**) associated with an electronic transition as follows;

¿

Where h is the Planck's constant (J.s) and v is the light frequency (s^{-1}). The value of exponent n represents the nature of electronic transition from valence band to conduction band.

The **Figure 5** shows the determination of the direct band gap of the samples by plotting $[F(R)h\upsilon]^n$ (n=2 for direct band gap) vs energy ($h\upsilon$). The line drawn at the linear part of $[F(R)h\upsilon]^2$ at $h\upsilon$=0 gives the value of band gap. The band gap values of the samples are inserted in **Table3**.

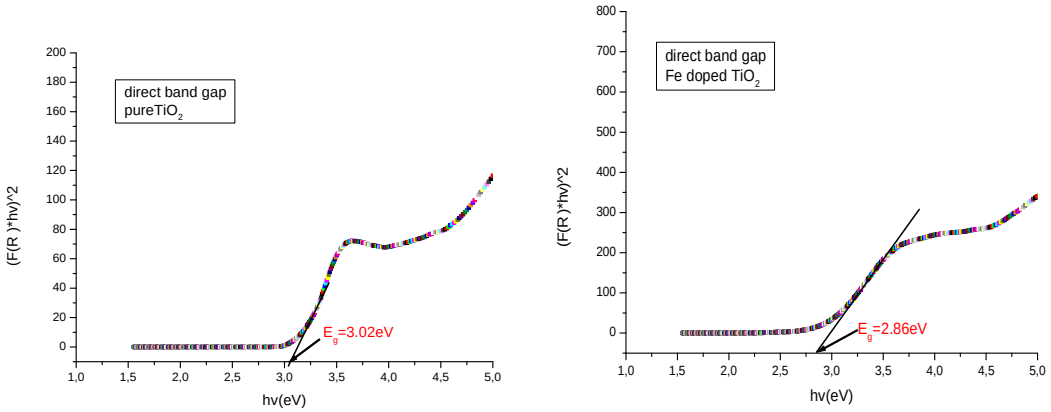

Fig. 5 shows the determination of the direct band gap for **a)** of pristine and **b)** doped TiO_2NPs by plotting $[F(R)h\upsilon]^{\wedge 2}$

The **Figure. 6** shows the determination of the indirect band gap of TiO_2 by plotting $[F(R)h\upsilon]^n$ (n=1/2 for indirect band gap) vs. energy ($h\upsilon$). The line drawn at the linear part of $[F(R)h\upsilon]^{1/2}$ at $h\upsilon$=0 gives the value of band gap. The values of the band gap of the samples are inserted in **Table3**.

Our results show that the band gap values estimated for the indirect transition are in agreement with the values obtained with the plotting absorption against wavelength, which confirme that the mixed phase samples exhibit an indirect electronic transition (indirect band gap. Obtained results are in accordance with Jin et Su results **[30, 19].**

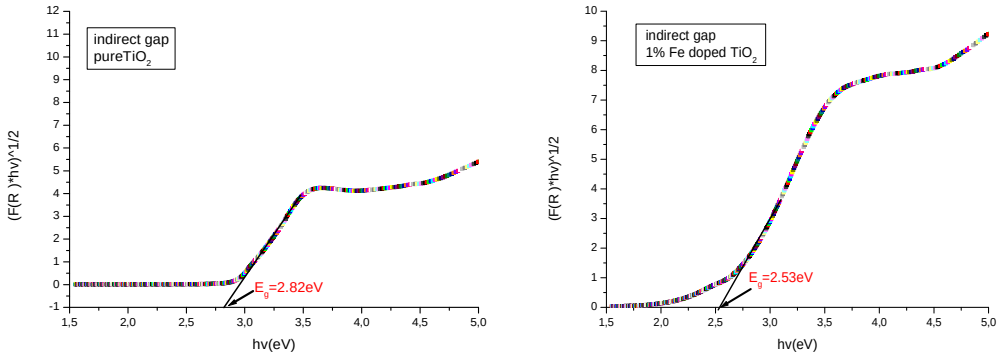

Fig. 6 Graphical representation of modified Kubelka–Munk function for **a)** undoped and **b)** doped TiO_2 by plotting $[F(R)hu]^{\wedge 1/2}$ versus hv

Table 3. Different values of Band gap energy estimated for pristine and Fe doped TiO_2 samples.

Samples	(F(R)hv)^2 (eV)	(F(R)hv)^1/2 (eV)	F(R) versus hv (eV)	F(R) versus λ (nm)
Pure TiO_2	3.02	2.82	2.81	440 (2.81eV)
Fe-TiO_2	2.86	2.53	2.53	489.60 (2.53eV)

4. Conclusion

In this paper, we have described the both band gap of nanocrystalline TiO_2 prepared by sol gel technique. A Comparison was made for optical property of pure and Fe doped TiO_2 NPs. Based on characterization results, all the produced samples are mixture phases and has lower indirect band gap, which corresponds to the visible region. We can conclude that sol gel, as a reproducible technique, is well adapted for the elaboration of high-quality of TiO_2 NPs with interesting structural and optical properties for photovoltaic application.

References

[1] Ao CH, Lee SC, Mak CL, Chan LY (2003) Photodegradation of volatile organic compounds (VOCs) and NO for indoor air purification using TiO_2: promotion versus inhibition effect of NO. Appl Catal B-Environ 42:119–129

[2] O'Regan B, Gratzel M (1991) A low-cost, high-efficiency solar cell based on dyesensitized colloidal TiO_2 films. Nature 353: 737–739.

[3] Sclafani A, Herrmann, J (1996) Comparison of the photoelectronic and photocatalytic activities of various anatase and rutile forms of titania in pure liquid organic phases and in aqueous solutions. J Phys Chem 100: 13655–13661.

[4] Munir S, Shah SM, Hussain H, khan RA (2016) Effect of carrier concentration on the optical band gap of TiO2 nanoparticles. Materials and Design 92 : 64–72

[5] Davis EA, Mott NF (1970) Conduction in non-crystalline systems V. Conductivity, optical absorption and photoconductivity in amorphous semiconductors. Philosophical Magazine 22: 0903– 0922.

[6] Nyankson E, Agyei-Tuffour B, Asare J Annan JE, Rwenyagila ER, Konadu DS, Yaya A, Dodoo-Arhin D (2013) Nanostructured TiO_2 and their energy applications -a review. J Engineering and Applied Sciences 8: 871-886.

[7] Zhang D, Chen J, Deng P Wang X, Li Y, Wen T, Li Y, Xiang Q, Liao Y (2019) Hydrogen evolution promotion of Au-nanoparticles- decorated TiO_2 nanotube arrays prepared by dip-loading approach. J American. Ceramic Society 102: 5873−5880.

[8] He Z, Kim C, Lin L, Jeon TH, Lin S, Wang X, Choi W (2017) Formation of heterostructures via direct growth CN on h-BN porous nanosheets for metal-free photocatalysis. Nano Energy 42: 58− 68.

[9] Pelaez M, Nolan NT, Pillai SC, Seery MK, Falaras P, Kontos AG Dunlop PSM, Hamilton JWJ, Byrne JA, O'Sheaf K, Entezari MH, Dionysiou DD (2012) A review on the visible light active titanium dioxide photocatalysts for environmental applications. Applied Catalysis B 125: 331–349.

[10] Chen H, Nanayakkara CE, Grassian VH (2012) Titanium Dioxide Photocatalysis in Atmospheric Chemistry. Chem. Rev 112: 5919–5948.

[11] Nyankson E, Agyei-Tuffour B, Asare J Annan JE, Rwenyagila ER, Konadu DS, Yaya A,

Dodoo-Arhin D (2013) Nanostructured TiO_2 and their energy applications -a review. J Engineering and Applied Sciences 8: 871-886.

[12] Munir S, Dionysiou DD, Khan SB, Shah SM, Adhikari B, Shah A (2015) Development of photocatalysts for selective and efficient organic transformations, J. Photochem. Photobiol. B 148: 209–222

[13] Liu X, Li Y, Deng D, Chen N, Xing X, Wang Y (2016) A one-step nonaqueous sol–gel route to mixed-phase TiO_2 with enhanced photocatalytic degradation of Rhodamine B under visible light. Cryst Eng Comm 18: 1964–1975.

[14] Paul S, Choudhury A (2014) Investigation of the optical property and photocatalytic activity of mixed phase nanocrystalline titania. Appl Nanosci 4: 839–847.

[15] Biswaji C, Bikash B, Amarjyoti C (2012) Extending Photocatalytic Activity of TiO_2 Nanoparticles to Visible Region of Illumination by Doping of Cerium. Photochemistry and Photobiology 88: 257-264.

[16] Hurum DC, Agrios AG, Gray KA, Rajh T, Thurnauer C (2003) Explaining the enhanced photocatalytic activity of degussa P25 mixed-phase TiO_2 using EPR. J Phys Chem B 107: 4545–4549

[17] Yamada Y, Kanemitsu, Y (2012) Determination of electron and hole lifetimes of rutile and nanatase TiO_2 single crystals. Appl Phys Lett 101: 133907.

[18] Baiju KV, Zachariah A, Shukla S, Biju S, Reddy MLP, Warrier KGK, (2009) Correlating photoluminescence and photocatalytic activity of mixed-phase nanocrystalline titania, Catal Lett. 130: 130–136.

[19] Su R, Ralf B, Lasse SR, Vang T, Michael S, Bjorn E, Anders P, Flemming B (2011) How the Anatase-to-Rutile Ratio Influences the Photoreactivity of TiO_2. J Phys Chem C 115: 24287–24292

[20] Zhu J, Zheng W, He B, Zhang J, Anpo M (2004) Characterization of Fe–TiO_2 photocatalysts synthesized by hydrothermal method and their photocatalytic reactivity for photodegradation of XRG dye diluted in water. J Mol Catal A 216: 35-43.

[21] Zhang YH, Reller A (2001) Nanocrystalline iron-doped mesoporoustitania and its phase transition. J Mater Chem 11: 2537-2541.

[22] Mokhtarimehr M, Akbar E, Mahmoud P (2013) Self-cleaning properties of Vanadium Doped TiO_2 sol-gel derived thin films. New J Glass Ceram 3: 34147-34150.

[23] Su C, Hong BY, Tseng CM (2004) Sol–gel preparation and photocatalysis of titanium dioxide. CatalysisToday 96: 119-126.

[24] Hirano M, Joji T, Inagaki M, Iwata H (2004) Direct formation of iron (III)-doped titanium oxide (Anatase) by thermal hydrolysis and its structural property. J Am Ceram Soc 87: 35-41

[25] D. Khudhair, A. Bhatti, Y. Li, H. Amani Hamedani, H. Garmestani, P. Hodgson, and S. Nahavandi, Mater. Sci. Eng. C 59, 1125 (2016).

[26] Y. Zhang, D. Yu, M. Gao, D. Li, Y. Song, R. Jin, W. Ma, and X. Zhu, Electrochim. Acta 160, 33 (2015).

[27] Tauc J, Grigorovici R, Vancu A (1966) Optical Properties and Electronic Structure of Amorphous Germanium. *Phys. Status Solidi B 15*: 627– 637.

[28] Mohammadnezhad F, Kampouri S, Wolff SK, Xu Y, Feyzi M, Lee JH, Ji X, Stylianou KC (2021)Tuning the Optoelectronic Properties of Hybrid Functionalized MIL-125-NH_2 for Photocatalytic Hydrogen Evolution. ACS Applied Materials &Interfaces *13:* 5044-5051 .

[29] Rosendo L and Ricardo G (2012) Band-gap energy estimation from diffuse reflectance measurements on sol–gel and commercial TiO2: a comparative study. J Sol-Gel Sci Technol 61: 1–7.

[30] Jing H, Yi-en D, Yang B, Jing A, Xuemei C, Yongqiang C, Pengfei W, Xiaojing Yang Y, Qi F (2019) Facile Formation of Anatase/Rutile TiO_2 Nanocomposites with Enhanced Photocatalytic Activity. J Molecules 24: 2996.

[31] Kasidid Y, Marcin K, Wojciech M TiO_2 with Tunable Anatase-to-Rutile Nanoparticles Ratios: How Does the Photoactivity Depend on the Phase Composition and the Nature of Photocatalytic Reaction", *ACS Applied Nano Materials***,** *4:* 633-643.

[32] Biswajit CAmarjyoti C (2013) Oxygen defect dependent variation of band gap, Urbach energy and luminescence property of anatase, anatase-rutile mixed phase and of rutile phases of TiO_2 nanoparticles", Physica E, 2013.